

Pressure-Force Transformation for Transient Wear Simulation in Two-Dimensional Sliding Contacts

Chen Y J^{1,2} and Huber N^{2,3}

Abstract: An efficient wear integration algorithm is crucial for the simulation of wear in complex transient contact situations. By rewriting Archard's wear law for two dimensional problems, the wear integration can be replaced by the total contact force. This avoids highly resolved simulations in time and space, so that the proposed method allows a significant acceleration of wear simulations. All quantities, including the average contact velocity, slip rate and total contact force, which are required for the pressure-force transformation, can be determined from geometric and motion analysis, or alternatively, from Finite Element simulations. The proposed CForce method has been implemented into the finite element based wear simulation tool Wear-Processor and was validated for a twin-wheel and a camshaft-follower model. A series of simulations have been carried out at high resolution. Resulting wear profiles from the conventional time integration approach and CForce method have been of excellent agreement. Further, it has been shown that the computation time can be significantly reduced. The simulation results from the CForce method remains robust against coarsening of the finite element mesh and increasing time increments.

Keywords: Wear, Wear prediction, Contact mechanics, Numerical simulation

1 Introduction

The ability to predict wear and lifespan is essential for the development of reliable engineering components, which are involved in tribo contacts. Manufacturing and

¹ Institut für Zuverlässigkeit von Bauteilen und Systemen, Universität Karlsruhe(TH), Kaiserstrasse 12, D-76131, Karlsruhe, Germany. Corresponding author. Tel: +49 (0)40-42878-4386; Fax: +49 (0)40-42878-4070; E-mail: yongjun.chen@tu-harburg.de

² Institut für Werkstoffphysik und Technologie, Technische Universität Hamburg-Harburg, Eißendorfer Strasse 42 (M), D-21073, Hamburg, Germany

³ Institut für Werkstofforschung, GKSS-Forschungszentrum Geesthacht GmbH, Max-Planck-Strasse, D-21052, Geesthacht, Germany

testing of prototypes is highly expensive both in terms of time and money. Numerical simulation has achieved increasing attention as an efficient way for wear prediction and component design.

For wear simulation, Archard's wear model is the most popular model as discussed by many authors (Strömberg 1999; Flodin and Andersson 2000; Williams 2001; Brauer and Andersson 2003; Sawyer 2004; Hegadekatte, Huber and Kraft 2005; Hegadekatte, Huber and Kraft 2005; Ding and Kahraman 2007; Dhanasekaran and Gnanamoorthy 2008; Hegadekatte, Hilgert, Kraft and Huber 2008; Nürnberg, Nürnberg, Golle and Hoffmann 2008; Zhao, Hilmas and Dharani 2009). Archard's wear law represents a linear relationship between the incremental wear, sliding distance and local contact pressure. A numerical simulation based on Archard's wear model for simulating the frictional wear behavior within a fully nonlinear kinematical setting including large slip and finite deformations is described by Strömberg (Strömberg 1999). Sawyer used a simulation scheme based on the Archard's wear model for the surface shape and contact pressure evolution during copper chemical mechanical polishing (Sawyer 2004). Brauer and Andersson proposed a mixed finite element simulation and analytical approach to simulate the wear in gears with flank interference, in which Archard's wear model is used (Brauer and Andersson 2003). An energy approach was proposed to simulate the wear occurring in deep drawing processes by Nürnberg (Nürnberg, Nürnberg, Golle and Hoffmann 2008). Recently, Zhao used a user subroutine based on Archard's wear model to investigate the wear behavior of a C/C composite multi-disk clutch under simulated operation conditions (Zhao, Hilmas and Dharani 2009).

A modified Holm-Archard wear law, that includes the effect of surface roughness, has been proposed by Liu et al. (Liu, Wriggers and Li 2004) in combination with a Node-to-segment Element. The approach has been demonstrated for indentation and a 2D pin-on-disk model. For the twin-disc and pin-on-disk models, the geometries are relatively simple and regular (Hegadekatte, Huber and Kraft 2005; Hegadekatte, Huber and Kraft 2005). In general, the geometry of the component is much more complicated in an industrial application, such as the conical involute, spur and helical gears (Flodin and Andersson 2000; Brauer and Andersson 2003; Ding and Kahraman 2007; Dhanasekaran and Gnanamoorthy 2008), micro-gears (Hegadekatte, Hilgert, Kraft and Huber 2010) and lobe pumps (Huber and Aktaa 2003), camshaft-follower systems (Hugnell, Björklund and Andersson 1996), coated systems (Steiner, Bouvier, May, Hegadekatte and Huber 2010) and so on.

In such situations the contact conditions change rapidly with time. In pioneering work, Andersson and co-workers implemented the Hertzian solution and the Winkler model on the local scale into the analytical model of a gear to resolve the local contact pressure distribution for wear integration (Flodin and Andersson 1997;

Fllodin and Andersson 2000).

As soon as multiple contacts and dynamic effects come into play, Finite Element simulations are so far the only possibility to achieve results, which correctly account for the local deformation in the context of the system behavior. An effort has been made recently, to capture the global and local behavior for wear simulation with a very fine meshed Finite Element model (Hegadekatte, Hilgert, Kraft and Huber 2008). The discrete nature of the finite element method implies that the time increments are sufficiently fine in order to resolve fast moving contacts and to achieve a correct integration of wear.

For life-span investigation, multiple wear steps are needed to predict the progress of wear that is changing the contact conditions on a very long time scale. All these conditions form a multi-scale problem in space and time causing a computation bottle-neck problem. Thus it is essential to develop an efficient approach for wear prediction, which accepts coarse finite element meshes and large time increments at high prediction accuracy.

Archard's law (Archard 1953) was originally formulated on the global component scale in the form

$$\frac{V_w}{s} = k_D F_N \quad (1)$$

with the wear volume, V_w , dimensional wear coefficient, k_D , sliding distance, s , and applied normal force F_N . To determine the local wear distribution in a tribosystem, commonly the local formulation

$$\frac{h}{s} = k_D p \quad (2)$$

is used, where p is the contact pressure at a point on the surface. For a further generalization towards sliding distance dependent or time dependent wear prediction, Eq.(2) needs to be formulated a differential equation (Brauer and Andersson 2003)

$$\frac{dh}{ds} = k_D p, \quad (3)$$

with which an initial value problem can be solved through integration over the loading history. The wear for each surface point results from the solution of the integral

$$h = k_D \int p ds = k_D \int p(t) \frac{ds}{dt} dt. \quad (4)$$

Equation (4) follows the concept of the single point observation method, which has been introduced by Andersson in (Andersson and Eriksson 1990). The Wear

Processor (Hegadekatte, Huber and Kraft 2005) solves this integral by an Euler integration scheme based on Finite Element results providing the data for the pressure and slip rate at each contact node. For quasi static cases, only the left hand integral of Eq. (4) needs to be solved for each wear increment, as it is for example the case for the pin in a pin-on-disc contact (Hegadekatte, Huber and Kraft 2005; Hegadekatte, Huber and Kraft 2005; Hegadekatte, Huber and Kraft 2006).

When the problem requires a fully transient integration as given by the right-hand side of Eq. (4), the time dependent pressure and slip rate needs to be stored for all potential contact nodes and for all time increments of the Finite Element simulation. In this case, data storage, data reading from the FEM output and integration of Eq. (4) consumes a tremendous part of the whole wear simulation time. Furthermore, the Finite Element model needs to be meshed very fine and time increments need to be sufficiently small. This is necessary to ensure that the pressure profile can accurately be resolved when the contact moves over a surface point. As a consequence, the numerical simulation does so far not allow simulating complex dynamic tribosystems. The only efficient solution for speeding up the wear simulation of a fully transient problem is currently parallel computing (Mukras, Kim, Sawyer, Jackson and Bergquist 2009).

The present work further develops an idea that has been proposed recently by Andersson (Andersson 2008). For the prediction of rolling and sliding wear in a 3D twin wheel configuration, Andersson simplified the problem by replacing the pressure profile, which a single point is experiencing, by the mean pressure derived from a Winkler surface. As emphasized in this work, the key for wear prediction is still to get the contact pressure field which is obtained directly from numerical simulation or from an analytical/empirical formulae (see also (Dhanasekaran and Gnanamoorthy 2008; Flores 2009)).

For generally shaped two dimensional tribo systems it is possible to replace the pressure integration by the contact force, as it will be shown in following, eliminating the necessity to determine the contact pressure field. A mathematical pressure-force transformation allows reducing the wear integration in Eq. (4) to a simple algebraic equation. This concept is similar to Eq. (1), but allows a space and time resolved wear prediction. Two cases of different complexity will be considered to validate the approach: a twin-wheel contact and a camshaft-follower system. The results confirm the potential of the new approach, which is more efficient and robust compared to the previous implementation of Eq. (4) presented in earlier work (Hegadekatte, Hilgert, Kraft and Huber 2008).

2 Pressure-force transformation

2.1 Theory

Corresponding to the single point observation method, Equation (4) integrates the product of the local contact pressure p and the slip rate ds/dt at a fixed surface point over time t , solving wear as an initial value problem. The concept of the pressure-force transformation is to modify the integral in such a way, that it reduces to $F_N = \int p dX$, where X is the tangential spatial coordinate and F_N is equivalent to the total contact force.

The slip rate ds/dt is given by the relative motion of the contacting surfaces and can be assumed to be constant when the contact area is small. This is true for Hertzian contacts. The relationship between time increment dt and space increment dX is defined by the current speed of the contact, v_c , relative to the surface point of the contacting body at a position X . With X being the tangential coordinate connected to the contacting body, we have $dX = v_c dt$.

Equation (4) can then be rewritten with the time increment $dt = dX/v_c$:

$$h = k_D \int p \frac{ds}{dt} dt = k_D \int p \frac{ds}{dt} \frac{dX}{v_c}. \quad (5)$$

With ongoing wear it is generally possible that the contact area is changing in size from point to point, which needs to be taken into account when the calculated wear is assigned to the surface nodes of a Finite Element model.

From view of a point at position x , which is involved in the contact only for a short period of time, we assume that changes in slip rate and contact velocity are sufficiently small and can be neglected, because they are only relevant as long as the contact pressure is non-zero. It is thus justified to write Eq. (5) in the form

$$h(x) = k_D \int p \frac{ds(x)}{dt} \frac{dX}{v_c(x)} = k_D \frac{ds(x)}{dt} \frac{1}{v_c(x)} \int p dX. \quad (6)$$

The integral term at the right-hand side of Eq. (6) is identical to the contact force. Thus the wear at an arbitrary location is directly related with the current values of slip rate, contact velocity, and contact force. Eq. (6) is only valid for two-dimensional Hertzian contacts, where the pressure profile is moving completely over a surface point with a non-zero contact velocity. This includes a number of technically important components, such as camshafts or gears, which are included in the class of plane rotating tribosystems.

In the first part of the paper we will validate our theory with a twin wheel model. Then we will show that the approach can be extended to more complicated cases,

such as a camshaft follower problem, where Eq. (6) will be applied to both camshaft and follower. For the outer regions of the follower, where the wear calculation by contact force is not allowed, Eq. (6) will be extended to obtain a correct solution.

2.2 Wear Processor implementation

The new method is implemented into the finite element based wear simulation tool, Wear-Processor 5.2, which has been described in detail in Refs (Hegadekatte, Huber and Kraft 2005; Hegadekatte, Huber and Kraft 2006). The change to the new version Wear-Processor 6.0, includes a number of improvements of which some are visible from the flow chart in Figure 1, The most important, relevant for this work, are explained below.

A) Contact variables

The latest version of ABAQUS 6.8.1 (ABAQUS 2008) provides the contact pressure p of the slave and master directly. Because the slip variable is provided only at the slave surface, the calculated slip rate needs to be interpolated to the master.

B) Numerical integration

To distinguish in the following between the conventional transient simulation with numerical integration and the new approach with pressure-force transformation, we denote the integration of Eq. (4) as “Ipdsdt” method, and the wear calculation by Eq. (6) as “CForce” method.

C) Large time increments

For the prediction of wear with the Ipdsdt method over the whole contact surface, the transient finite element simulation is forced to a very small time increment. With the CForce method an interpolation algorithm is introduced, which is sketched in Figure 2. At large time increments a number of surface nodes are left out in the wear calculation. It is possible to interpolate the result to these nodes, as indicated in Figure 2. The basis for the linear interpolation can be any coordinate x or θ describing uniquely the position of the surface nodes relative to each other.

The linear interpolation can be described as following,

$$h_w(x) = h_{w1} + \frac{x - x_1}{x_2 - x_1} (h_{w2} - h_{w1}). \quad (7)$$

The interpolation is simply linear and can handle only stable contact situations. Jumps or high gradients, which can occur by different reasons, such as dynamics of the system or in multi-contact situations, need to be treated carefully as this is the case for Finite Element simulations without wear. If the solution is not sufficiently stable, a refinement of the time stepping in the relevant region is suggested.

D) Python control

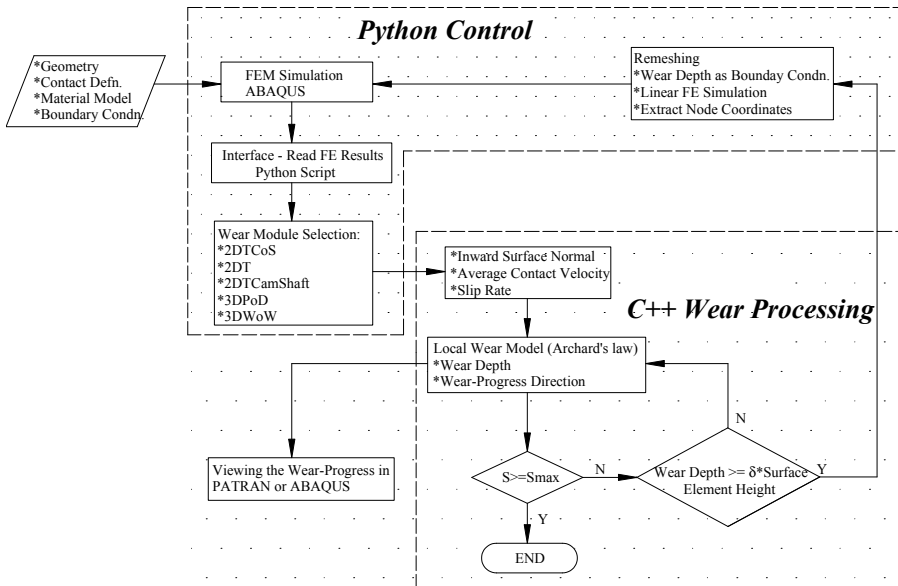


Figure 1: Flow chart for the working of Wear-Processor 6.0

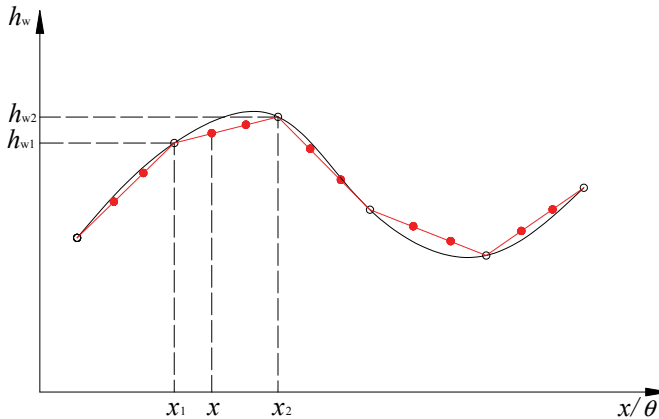


Figure 2: Interpolation of wear over the contact surface for large time increments

The flow chart is separated into two parts; the python control part and the C++ wear processing part. Preparation and starting of the contact simulation, reading FE results interface, wear module calling, and re-meshing process are integrated in the python control part. The C++ part of the code includes all time

consuming operations in form of various modules, which are needed for the wear calculation of a specific configuration. The different modules can be selectively called from the Python control depending on the problem to be solved. Applications with the respective modules have been published earlier for 3D pin-on-disc (Hegadekatte, Huber and Kraft 2005; Hegadekatte, Huber and Kraft 2006), twin wheel tribometer (Hegadekatte, Huber and Kraft 2005), 2D gear tooth and cylinder-on-slab (Hegadekatte, Hilgert, Kraft and Huber 2008).

3 Twin-wheel

For validation of the CForce implementation in the Wear Processor a 2D twin-wheel model is considered as shown in Figure 3. The radii of the top cylinder and the bottom cylinder are R_1 and R_2 , and the angular velocities are ω_1 and ω_2 , respectively. The bottom cylinder can only rotate around its geometric center, while only the horizontal freedom is constrained for the top cylinder. Thus it can not only rotate around its center, but also move in vertical direction to compensate wear. A downward external loading F_N is applied at the center of the top cylinder. The contact length is $2a$.

The detailed configuration of the top cylinder is shown in Figure 4. For an arbitrary point A on the outer surface, the corresponding angle related to the initial vertical line OM is defined as θ , and the angle of the half contact length a related to the geometric center O is defined as ψ .

An analytical solution of Eq.(6) can be obtained from geometric and motion analysis in analogy to (Andersson 2008).

3.1 Scaling laws

The following dimensional analysis can be applied to both the twin-wheel and camshaft follower model. The dependent variable is the wear h_w . The independent variables are the radius of the wheel or wheel/camshaft R , eccentric distance d , external loading F_N , dimension wear coefficient k_D , Young's modulus E and the number of rotations N . The corresponding dimensions of these variables are listed in Table 1. For a full description of the twin-wheel configuration, another pair of radius and number of rotations needs to be included for the second wheel. This would add no more physics into the dimensional analysis and is omitted here.

Using the Buckingham Π -theorem, we can derive from the 7 dimensional variables 5 dimensionless variables, which are $h_w/(k_D F_N)$, d/R , $F_N/(ER)$, $k_D E$, and N . As long as wear is small, compared to the dimension of the cylinder $h_w \ll R$, the wear depth h_w increases linearly with the number of rotations N . This combines the two dimensionless variables $h_w/(k_D F_N)$ and N in a single dimensionless variable

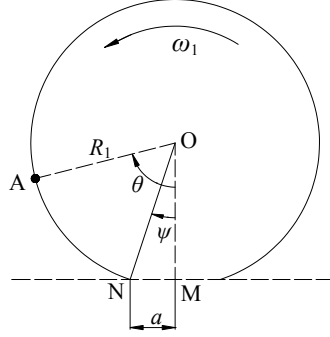
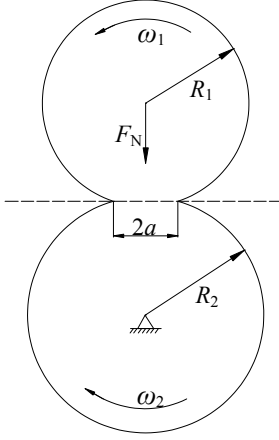


Figure 3: Configuration of the twin-wheel model Figure 4: The details of the top cylinder

Table 1: Dimension of dependent and independent variables in the 2D case (the normal force is considered as force per unit depth)

	h_w	R	d	F_N	k_D	E	N
N	0	0	0	1	-1	1	0
mm	1	1	1	-1	2	-2	0

$h_w/(k_D F_N N)$. As a result, the most important dependencies are expressed in a relationship between dimensionless variables as given by

$$h_w^* = \frac{h_w}{k_D F_N N} = f\left(\frac{d}{R}, \frac{F_N}{ER}, Ek_D\right). \quad (8)$$

From Eq. (8) we can conclude in the first approximation, that the amount of wear is proportional to the dimensional wear coefficient, external load, and number of rotations. For the twin-wheel configuration, the parameter $d/R \equiv 0$; in the camshaft-follower configuration this parameter describes the influence of the eccentricity on wear (see Sect. 4 for details).

The parameter $F_N/(ER)$ is a measure for the elastic deformation and defines the half contact length a in Figure 4. The dimensionless material parameter $k_D E$ describes the influence of elastic deformation on the local distribution of wear. Earlier work has shown, that the wear distribution is only affected by elastic deformation if the material is very soft (Polymers, Rubber) (Hegadekatte, Huber and Kraft 2006).

For the comparison of the different approaches applied throughout this work, it is useful to present the results for dimensionless wear $h_w^* = h_w / (k_D F_N N)$ as a local distribution along the contact surface. For the purpose of validation the restriction to results calculated for the initially unworn surface is sufficient, which is equivalent to omitting the number of rotations in function $f(\cdot)$ of Eq. (8).

3.2 Analytical solution for the twin-wheel model

During one rotation, the contact length $2a$ as well as the contact position in the global coordinate system remains constant. For the top cylinder in Figure 4, each surface node will pass the contact zone once. When point A reaches position N , the contact pressure p is positive for the first time, and when it reaches position M after a time interval Δt , it has passed half of the contact pressure profile. When the contact area is small, the contact velocity reduces to $v_c^{top} = \omega_1 R_1$ for the top cylinder and $v_c^{bot} = \omega_2 R_2$ for the bottom cylinder, respectively.

The slip rate between the top and bottom cylinders is given by:

$$\frac{ds}{dt} = \omega_1 R_1 - \omega_2 R_2. \quad (9)$$

The different rotation frequency of the two wheels causes an unequal number of rotations during the simulation. Generally, if a cylinder rotates N turns in the contact simulation; this effect will be taken into account by

$$h_w(\theta) = \frac{1}{v_c(\theta)} \frac{ds(\theta)}{dt} k_D N F_N. \quad (10)$$

From Eq. (10), the wear of the top and the bottom cylinder can be derived analytically corresponding to their specific number of rotations during a given period of time.

3.3 Validation of Wear-Processor implementation

For the validation of the CForce implementation in the Wear Processor, a twin wheel finite element model has been generated that contains 41218 nodes and 34340 elements. For one wear step, the contact simulation takes 54:35 minutes on a computer with 4 duo-core CPUs and 8 GB Memory.

The external force on the top wheel is $F_N=23$ N. Related to earlier work (Hegadekatte, Hilgert, Kraft and Huber 2008) the outer radii of the slave (bottom cylinder) and master (top cylinder) are 1.183mm and 1.014mm, respectively. Both the dimensional wear coefficients for the top and bottom cylinders are 13.5×10^{-9} mm³/Nmm.

The angular velocities of the slave and master are 12.566 rad/s and 6.283 rad/s, respectively. With the total rotation time of 1 second, slave and master rotate for 2 and 1 turn, respectively.

In this simulation, the total rotation time is 0.025 seconds, and the angles of the non-zero wear zone for the slave and master are 18 degree and 9 degree, respectively. The nodes, which are included by these angles, experience the contact only one time. The comparison of the results for both cylinders is shown in Figure 5 and Figure 6, respectively.

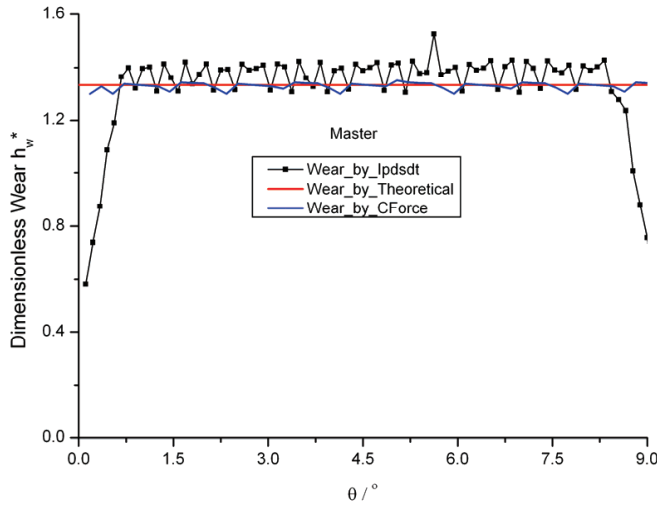


Figure 5: Results from the analytical solution (10) and the Wear Processor (Ipdsdt, CForce) for the master cylinder.

The dimensionless wear for each point on the master and the slave surface is $h_w^* = 1.333$ and $h_w^* = 0.571$, respectively. It can be seen from Figure 5 and Figure 6 that the CForce method achieves a higher accuracy and robustness compared to the Ipdsdt method. The stability of the CForce method is originating from the insensitivity of the global force with respect to the spatial resolution of the pressure profile. The remaining oscillations are mainly due to the tolerance for solving the equilibrium conditions with the contact algorithm and can be further reduced by adjusting the corresponding parameter in ABAQUS.

The results from Ipdsdt method show a sharp drop at both ends. This can be explained by the integration $\int p ds$ in Eq. (4). Nodes in the surface region near to $\theta=0^\circ$ just go through about half of the contact length, and therefore, the wear is lower than in regions which pass the full contact length.

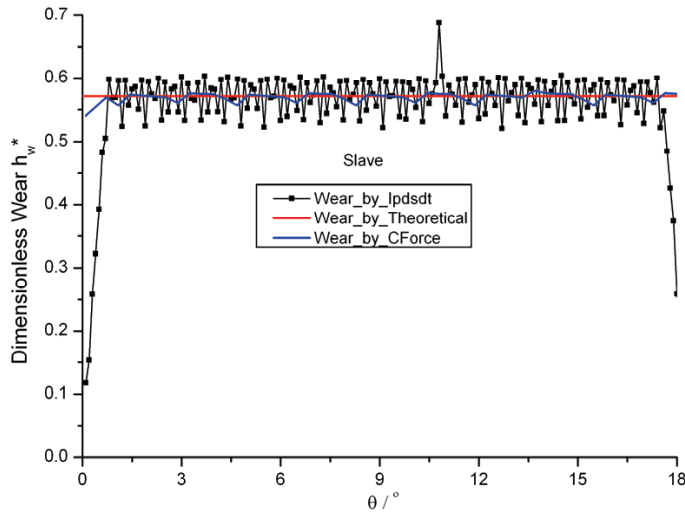


Figure 6: Results from the analytical solution (10) and the Wear Processor (Ipdsdt, CForce) for slave cylinder

With the choice of this model, we have a special case, where the contact itself is not moving in space. This is however the case for many technical applications. To proof, that Eq. (6) holds also for problems with a moving contact, we will extend our investigation to a simplified camshaft-follower model in the next step.

4 Camshaft follower

For further validation of the CForce method with a moving contact, a simplified camshaft follower configuration has been chosen. In technical applications, the camshaft geometry consists of several segments of different shape. Here, the simplest case of a cylinder with an eccentric axis of rotation is used.

The configuration of the camshaft follower model is shown in Figure 7. The radius of the top camshaft is R , and the angular velocity is ω . The camshaft is rotated around the fixed point A; the distance from the rotation center A to the geometric center O of the camshaft is denoted by d . The bottom follower can move only in vertical direction, and an upward external load, F_N , is applied in the center of its bottom surface. The total Hertzian contact length is $2a$.

When the geometric center O of the camshaft is above point A, the corresponding angle θ is zero; when point O is below point A, the corresponding θ is equal to 180° . A more detailed description of the motion is shown in Figure 8 for two times

t_1 and t_2 .

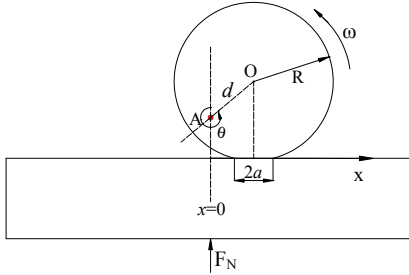


Figure 7: Configuration of a simplified camshaft-follower model: circular camshaft rotating around point F with vertically moving plate as follower

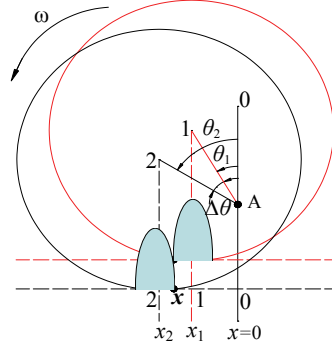


Figure 8: The details of the motion of the circular camshaft for time points $t_0 = 0, t_1 > t_0$ and $t_2 > t_1$

4.1 Analytical solution of the camshaft follower model

4.1.1 Wear of the camshaft

The contact velocity for the camshaft is defined from its sliding against the horizontally fixed follower by

$$v_c = \omega R. \tag{11}$$

From the geometry shown in Figure 8 we can derive the slip rate

$$\frac{ds(\theta)}{dt} = \omega (R - d \cos \theta). \tag{12}$$

Inserting Equations (11) and (12), into Eq. (10), the wear of camshaft can be expressed as

$$h_{w, \text{Camshaft}}(\theta) = k_D N F_N \left(1 - \frac{d}{R} \cos \theta \right). \tag{13}$$

4.1.2 Wear of the follower

The variable describing the position of the surface nodes of the follower is the coordinate x , see Figure 8. When the camshaft rotates for N turns, all nodes of the

follower in the region $x \in [-(d-a), (d-a)]$ will be subjected to N times left and right motion. From Eq. (6) follows that

$$h_{w, \text{Follower}}(x) = k_D \left(\frac{1}{v_{c, \text{left}}(x)} \frac{ds_{\text{left}}(x)}{dt} + \frac{1}{v_{c, \text{right}}(x)} \frac{ds_{\text{right}}(x)}{dt} \right) \times NF_N. \quad (14)$$

It should be noted, that surface points in the outer regions of the follower $|x| \in [(d-a), (d+a)]$ experience only a part of the passing pressure profile. Particularly points at positions $d < |x| < d+a$ experience a non-zero wear due to the extension of the contact area. Wear in this region would be ignored by assuming a point contact (see. Figure 8).

The partial pass can be corrected by introducing an effective contact force factor, $\xi(x)$:

$$h_{w, \text{Follower}}(x) = k_D \left(\frac{1}{v_{c, \text{left}}(x)} \frac{ds_{\text{left}}(x)}{dt} + \frac{1}{v_{c, \text{right}}(x)} \frac{ds_{\text{right}}(x)}{dt} \right) \times NF_N \times \xi(x). \quad (15)$$

The slip rate is given by Eq. (12) from the camshaft surface. For a position x on the follower, the central angle is θ and $(\pi - \theta)$ when the camshaft moves left and right, respectively. Inserted in Eq. (12), we obtain

$$\frac{ds_{\text{left}}(x)}{dt} + \frac{ds_{\text{right}}(x)}{dt} = \omega(R - d \cos \theta) + \omega(R - d \cos(\pi - \theta)) = 2\omega R. \quad (16)$$

Due to the symmetry, the absolute value of the contact velocity should equal in both directions, i.e. $v_{c, \text{left}}(x) = v_{c, \text{right}}(x)$. In order to determine the contact velocity $v_c(x)$ for the follower, we consider the motion presented in Figure 8. In the centre region of the follower, the contact velocity could be derived simply by assuming that the contact area is reduced to a point under the centre O of the camshaft as $v_c \approx \omega d |\cos \theta|$. However, the situation changes as soon as the outer edge of the contact approaches the point $|x| = d - a$. Then the extension of the contact becomes relevant and we have to introduce an average contact velocity calculated from the individual velocities of the two contact edges, as described in the following.

As it can be seen in Figure 8, the contact pressure profile reaches first the position x , when the camshaft center O is at position x_1 at time t_1 . When the contact pressure profile leaves the position x , the camshaft center O is located at x_2 , and the corresponding time is t_2 . From time t_1 to time t_2 , the contact has moved a distance $\Delta l = 2a$ over the point x during the time interval $\Delta t = t_2 - t_1 = \Delta \theta / \omega = (\theta_2 - \theta_1) / \omega$. Inserted in $v_c(x) = \Delta l / \Delta t$, with $\theta_1 = -\arcsin(x_1/d)$ and $\theta_2 = -\arcsin(x_2/d)$, the

average contact velocity for the point x is

$$v_c(x) = \frac{(x_1 - x_2) \omega}{\arcsin(x_1/d) - \arcsin(x_2/d)}. \quad (17)$$

For the analytical model we assume that the contact length $2a$ remains constant during the rotation. In the numerical implementation this will not be true after some wear has taken place so that the contact length will be derived from the contact simulation for each time increment. Note that for the following discussion, d is not allowed to be smaller than $2a$. Consequently, there is always a region, which is exposed to the full pressure profile excluding an application of our model to fretting wear.

For the calculation of the average contact velocity we have to consider two cases. In the inner region $|x| \leq d - a$ both contact edges contribute to the average contact velocity. Inserted in Eq. (17) we have

$$v_c(x) = \frac{2a\omega}{\arcsin((x+a)/d) - \arcsin((x-a)/d)}. \quad (18)$$

In the outer region $d - a < |x| \leq d + a$ only a part of the pressure profile moves over surface point x and the experienced distance reduces to $\Delta l = d + a - |x| < 2a$. For the resulting increment Δl , the average contact velocity is then given by:

$$v_c(x) = \frac{(d + a - |x|)\omega}{\pi/2 - \arcsin((|x| - a)/d)}. \quad (19)$$

The effective contact force factor $\xi(x)$, which is needed to correct the total contact force to the partial pass of the pressure profile at such a surface point $|x| > d - a$, can be obtained from integration of the elliptical pressure distribution. Due to symmetry, we get:

$$\begin{aligned} \xi(x) &= \frac{\int_{|x|}^{d+a} \sqrt{1 - ((|x| - d)/a)^2}}{\int_{d-a}^{d+a} \sqrt{1 - ((|x| - d)/a)^2}} \\ &= \frac{1}{2} - \frac{1}{\pi} \left(\arcsin \frac{|x| - d}{a} + \frac{|x| - d}{a} \sqrt{1 - \left(\frac{|x| - d}{a} \right)^2} \right). \end{aligned} \quad (20)$$

From Equations (12), (14)-(16) and (18)-(20), the wear of the follower can be determined analytically.

4.2 Wear-Processor simulation

The dimensionless parameters used for the finite element simulation were $d/R = 0.5$, $F_N/(ER) = 3.29 \times 10^{-3}$, and $k_D E = 4.104 \times 10^{-3}$. The angular velocity of the camshaft is 6.283 rad/s. Both the dimensional wear coefficients for the camshaft and follower are $13.5 \times 10^{-9} \text{ mm}^3/\text{Nmm}$, friction was not considered. The effect of friction was studied by varying the friction coefficient from $\mu = 0$ to $\mu = 0.45$. The effect in the simulated wear was negligible small compared to other numerical uncertainties. We observed a slight shift of the wear peak against the direction of surface traction by one top surface element length, which is a small percentage of 1.56% of the camshaft radius. The friction coefficient was thus set to zero for all following simulations.

The numerical model is shown in Figure 9. The model contains 4719 nodes and 4116 elements. A relatively high normal force has been applied in order to create a large contact area, which is needed to visualize the specific wear behavior in the outer contact region. In this example, the time increment for the contact simulation has been fixed at 0.005 s. For one wear step, the contact simulation took 13 minutes. The total computation time for one wear step is 32 and 29 minutes for the Ipdst and the CForce method, respectively. Because the Finite Element model and the chosen time increments are identical for both methods, only a small time saving of only 10% results from the reduced data processing and the elimination of the time integration with the CForce method. About 50% of the computing time is consumed by the finite element simulation.

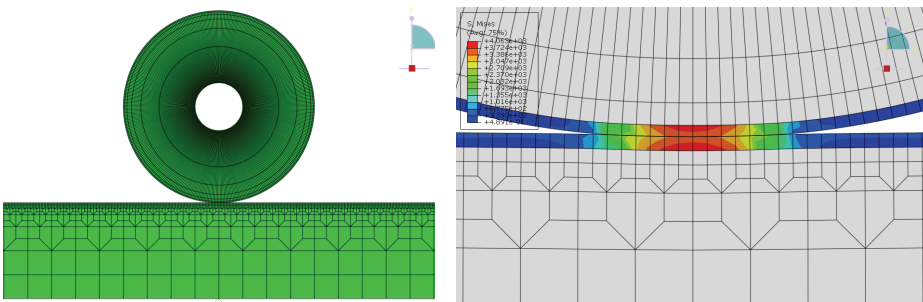


Figure 9: Finite element model for the camshaft-follower

The dimensionless wear $h_w^* = h_w/(k_D F_N N)$ is shown in Figure 10 and Figure 11 for the camshaft and follower, respectively.

It can be seen that the wear distributions for the camshaft and the follower coincide excellently for all three methods. The agreement with the Ipdst method validates

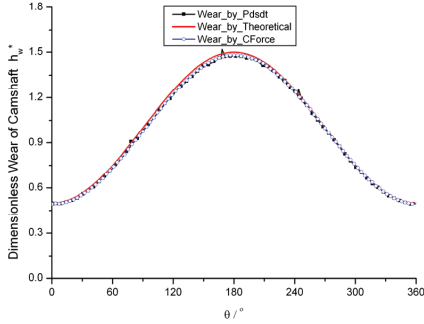


Figure 10: Wear of the camshaft

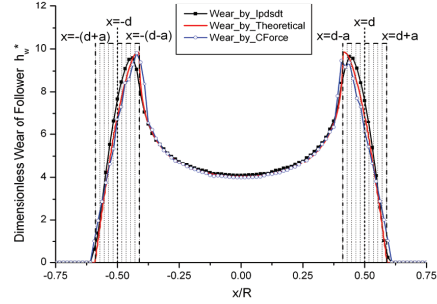


Figure 11: Wear of the follower

both the CForce method and the analytical solution. The small differences at the maximum value of the follower's wear at $|x|=d-a$ are the result of the finite elements, which are equally meshed over the whole follower surface. With a finer mesh in the peak region, the deviation would further reduce.

Comparing the wear results in Figure 10 with those in Figure 5 and Figure 6, which show a constant wear, we can see the influence of the eccentricity $(1 - d/R \cdot \cos \theta)$ of the camshaft. Maximum wear occurs at $\theta=180^\circ$, where the point O is just below the point A, i.e. the slip rate has its highest value. The minimum wear occurs at $\theta=0^\circ$, where the point O is just above point A, where the slip rate reaches a minimum (see Figure 7).

For the follower, the wear distribution assumes a very interesting shape, which looks like a saddle. The wear of the surface node is zero for $|x| > d + a$, because such points do not enter into the contact. While $|x|$ increases from 0 to $(d + a)$, the wear firstly increases until the position $|x| = d - a$ is reached.

Then, the pressure profile does not fully pass the surface nodes any more and the wear decreases until the outermost contact point $|x| = d + a$ is reached. Thus, wear caused by the extended contact area results in a characteristic drop of wear in the outer regions $|x| > d - a$ as it can be seen from Figure 11. This phenomenon can be understood from Eqs. (14) and (15) in more detail. When $|x|$ increases from 0 to $(d - a)$, the average contact velocity $v_c(x)$ in the denominator decreases and hence the wear increases gradually. When $|x|$ increases from $(d - a)$ to $(d + a)$, the average contact velocity still decreases to zero, but then the effective contact force factor $\xi(x)$ in Eq. (15) decreases much faster and the wear is brought to zero.

From Figure 10 and Figure 11, we can see that the maximum dimensionless wear is 1.5 and 9.85 for the camshaft and the follower, respectively. The difference of almost one order of magnitude can be explained from Eqs. (11) and (18). The

average contact velocity of camshaft and the follower is 1.255 mm/s and 0.257 mm/s, respectively, at the position $|x| = d - a$. Because the average contact velocity is much smaller for the follower, it wears faster according to Eq. (6). In other words, the fast rotating camshaft mills the follower surface away, while the contact moves slowly along the follower back and forth twice per rotation.

5 Results and discussion

5.1 Multiple wear steps

In this section, the simulation is carried out with the same parameters as in section 4.2. The total computation time for 210 turns (6 wear steps) is 3:12h and 2:49 h with the Ipdstdt and the CForce method, respectively. The progress of wear for the camshaft and follower are shown in Figure 12 and Figure 13, respectively. The wear depth is presented normalized in the form h_w/R in order to visualize the wear progress in relation to the dimension of the camshaft during multiple wear steps.

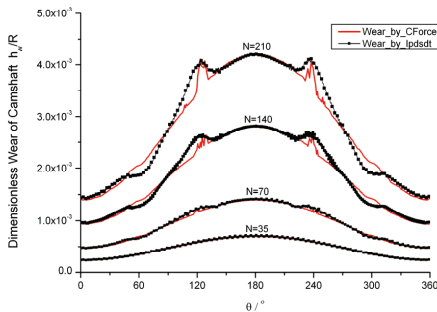


Figure 12: Wear progress of the camshaft for 210 rotations, calculated with 6 wear steps

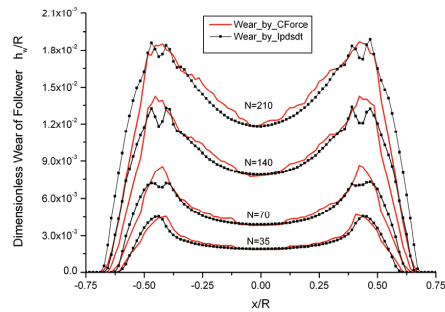


Figure 13: Wear progress of the follower for 210 rotations, calculated with 6 wear steps

The wear calculated by Ipdstdt and CForce methods are in good quantitative agreement for the most part of the worn surface. The ratio between the maximum wear and the minimum wear is 2.983 and 2.981 for the 1st and the 6th wear step, respectively. This ratio remains the same during the wear progress, supporting the conclusions from the dimensional analysis Eq.(8).

During the different wear steps, the wear distribution on the camshaft surface shows however several interesting characteristics. After several wear steps, the wear distribution is no longer as smooth as that in the first wear step. This is a result of the fast wear of the follower, which significantly changes the contact conditions

(pressure and contact area) depending on the position x . An example after the 6th wear step is shown in Figure 14. This effect leads to some qualitative discrepancies between the two methods in the local distribution of the wear profile between 60° and 120° as well as between 240° and 300°.

For both bodies the calculated wear from the two different methods is comparable in every wear step, i.e. there are no errors that may sum up over multiple wear steps. The region on the follower surface, where the wear is non-zero, grows with the increasing of the wear step from the camshaft digging into the follower surface.

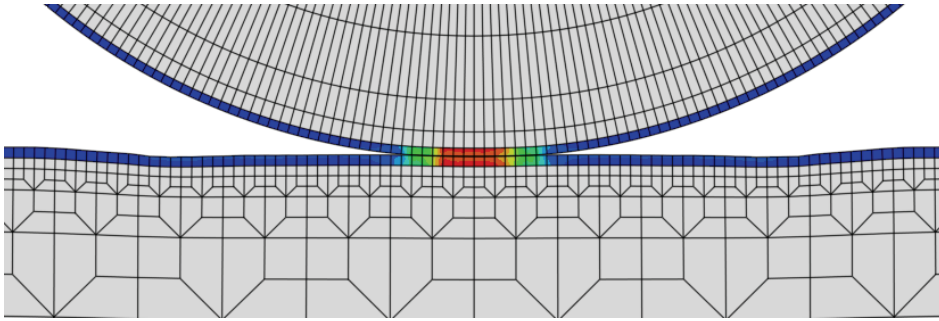


Figure 14: Shape of the follower after the 6th wear step

From Figure 14 it can be seen that the surface of the follower shows a significant amount of wear after 6th wear step. The two concave positions in the follower result from the two positions of maximum wear at $|x/R| \approx 0.4$ in Figure 13. The convex regions correspond to the positions of reduced wear in the centre and the outer regions.

Concerning the wear on the camshaft in Figure 12, we can assume that the slip rate and average contact velocity is not much affected by the progressing wear of the system. When the camshaft passes through the convex areas at angular positions of 120°, 180°, and 240°, the increased contact pressure leads to locally higher wear rate, while in the concave – and therefore more conforming – contact positions at 60° and 300°, the wear rate is reduced with respect to the theoretical cosine behavior.

After 210 turns of the camshaft, the maximum wear of the camshaft and the follower is about 0.42% and 1.87% of the camshaft radius R , respectively. Using the scaling law Eq. (8), this amount of wear will be constant for any combination of parameters $k_d F_N N = 5.67 \cdot 10^{-4}$ used for this simulation. If 0.4% would be the maximum tolerable wear, for example calculated from the thickness of a DLC-coating on the camshaft, the critical combination of $k_d F_N$ can be easily calculated

for a given lifetime of the coating N .

5.2 Benchmarking of the methods

To demonstrate the potential of the CForce method, the simulation is repeated with the same model but with an increased time increment of $\Delta t=0.015$ s. This is a factor three compared to Section 5.1. For one wear step, the contact simulation takes now 7.2 minutes. The total computation time for 210 turns (6 wear steps) is 1:49 h and 1:37 h with the Ipdstdt and the CForce method, respectively. Thus the total computation time has been reduced by 43%. This case is used as a first example to study the feasibility of the CForce and Ipdstdt method when the time is chosen such that the contact movement per time increment exceeds more than one surface element.

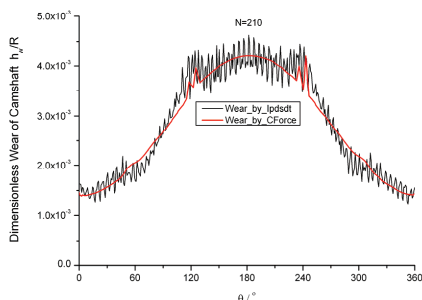


Figure 15: Accelerated wear simulation results for the camshaft

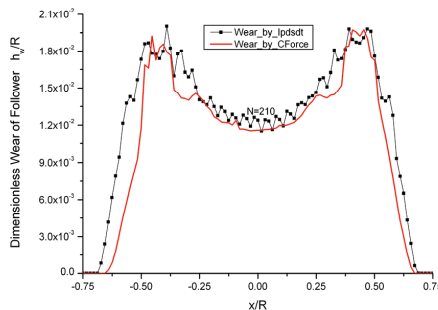


Figure 16: Accelerated wear simulation results for the follower

At such a large time increment, the wear distribution of camshaft calculated by Ipdstdt method shows significant oscillations. This leads to an artificial roughening and does not allow for wear prediction with multiple wear steps. The wear distribution for the follower calculated by the Ipdstdt method also oscillates in the center zone but shows good results in the other regions.

The observed oscillations can be understood from the integration of contact pressure over slip distance $\int pds$. When the time increment becomes too large, the pressure profile is not complete for many surface nodes. Thus, the wear integration shows large variations depending how much information on the pressure profile and slip information has been registered for a specific surface position. For nodes, for which only a part of the pressure profile is available, the integrated amount of wear is only a proportion of the correct wear, and then the wear distribution oscillates heavily.

In the case of the follower, the contact moves in the center zone much faster than in the outer zone. Only a part of the surface nodes in the center zone can see the correct pressure profile, and hence the computed wear oscillates. In the outer zone, the contact moves slowly, compared to the nodes in the center zone and the pressure profile is still complete. Hence, the wear distribution is smoother than in the center zone.

Through the combination of the CForce method with the interpolation of wear over the surface as shown in Figure 2, the Wear Processor can easily obtain a smooth wear curve for the camshaft. Even some complex details are still retained in the wear distribution. We can assume that for much larger time increments, such details may disappear, but the prediction of the general wear behavior will still be correct. Therefore, the CForce method can be applied in connection with large time increments with sufficient accuracy and with significantly reduced computation time.

6 Conclusion and outlook

A method for prediction of wear has been proposed, which is based on contact force. It has been shown for a twin-wheel model and a simplified camshaft-follower configuration that the so-called CForce method can achieve excellent results, compared with the conventional Ipdst approach. The CForce method uses an interpolation algorithm, which ensures that the correct wear can be assigned to un-contacted nodes and, thus, it is still feasible for wear predictions when the time increment in the contact simulation is significantly increased.

The goal of our future work is to implement this methodology to predict the life-span of realistic engineering components. Because the CForce method is robust for coarse finite element meshes, it has the potential to further reduce the computation time by more than a factor of 10. It furthermore represents an efficient approach based on finite element simulations, which allows accounting for the elastic deformation of a system as well as dynamic effects. In this way, the present work opens up new possibilities to solve complex systems, such as gears or realistic camshaft-follower configurations, with sufficient accuracy and within a limited computation time. It can be easily extended to multiple contact situations. In further work also the possibilities will be investigated for an extension to 3D problems, as they are occurring in piston cylinder contacts or in hip joints.

Acknowledgement: The authors would like to thank the German Research Foundation (DFG) for funding this work under transfer project T3 within the scope of the collaborative research center, SFB 499 – Design, production and quality as-

surance of molded micro-parts constructed from metals and ceramics. The authors would like to thank Vishwanath Hegadekatte for his fruitful work during his research for sub project D3 as well as Sören Andersson for his valuable comments and suggestions.

References

- ABAQUS** (2008): Version 6.8.1, Dassault Systemes Simulia Corp.
- Andersson, S.** (2008): Wear simulation with a focus on mild wear in rolling and sliding contacts. *Proceedings DGM Symposium*, Aachen, Germany.
- Andersson, S.; Eriksson, B.** (1990): Prediction of the sliding wear of spur gears. *Proceedings of NORDTRIB*, Hirthshals, Denmark.
- Archard, J. F.** (1953): Contact and rubbing of flat surfaces. *Journal of Applied Physics*, 24(8), pp.981-988.
- Brauer, J.; Andersson, S.** (2003): Simulation of wear in gears with flank interference - a mixed FE and analytical approach. *Wear*, 254(11), pp.1216-1232.
- Dhanasekaran, S.; Gnanamoorthy, R.** (2008): Gear tooth wear in sintered spur gears under dry running conditions. *Wear*, 265(1-2), pp.81-87.
- Ding, H. L.; Kahraman, A.** (2007): Interactions between nonlinear spur gear dynamics and surface wear. *Journal of Sound and Vibration*, 307(3-5), pp.662-679.
- Flodin, A.; Andersson, S.** (2000): Simulation of mild wear in helical gears. *Wear*, 241(2), pp.123-128.
- Flodin, A.; Andersson, S.** (1997): Simulation of mild wear in spur gears. *Wear*, 207(1-2), pp.16-23.
- Flores, P.** (2009): Modeling and simulation of wear in revolute clearance joints in multibody systems. *Mechanism and Machine Theory*, 44(6), pp.1211-1222.
- Hegadekatte, V.; Hilgert, J.; Kraft, O.; Huber, N.** (2010): Multi time scale simulation for wear prediction in micro-gears. *Wear*, 268(1-2), pp.316-324.
- Hegadekatte, V.; Huber, N.; Kraft, O.** (2005): Development of a simulation tool for wear in microsystems, Wiley VCH, Weinheim.
- Hegadekatte, V.; Huber, N.; Kraft, O.** (2005): Finite element based simulation of dry sliding wear. *Modelling and Simulation in Materials Science and Engineering*, 13(1), pp.57-75.
- Hegadekatte, V.; Huber, N.; Kraft, O.** (2006): Modeling and simulation of wear in a pin on disc tribometer. *Tribology letters*, 24(1), pp.51-60.
- Huber, N.; Aktaa, J.** (2003): Dynamic finite element analysis of a micro lobe pump. *Microsystem Technologies*, 9(6-7), pp.465-469.

Hugnell, A.; Björklund, S.; Andersson, S. (1996): Simulation of the mild wear in a cam-follower contact with follower rotation. *Wear*, 199(2), pp.202-210.

Liu, F.; Wriggers, P.; Li, L. J. (2004): Wear simulation based on node-to-segment element. *Key Engineering Materials*, 274-276, pp.577-582.

Mukras, S.; Kim, N. H.; Sawyer, W. G.; Jackson, D. B.; Bergquist, L. W. (2009): Numerical integration schemes and parallel computation for wear prediction using finite element method. *Wear*, 266(7-8), pp.822-831.

Nürnberg, K. E.; Nürnberg, G.; Golle, M.; Hoffmann, H. (2008): Simulation of wear on sheet metal forming tools - An energy approach. *Wear*, 265(11-12), pp.1801-1807.

Sawyer, W. G. (2004): Surface shape and contact pressure evolution in two component surfaces: Application to copper chemical mechanical polishing. *Tribology letters*, 17(2), pp.139-145.

Steiner, L.; Bouvier, V.; May, U.; Hegadekotte, V.; Huber, N. (2010): Modelling of unlubricated oscillating sliding wear of DLC-coatings considering surface topography, oxidation and graphitisation. *Wear*, 268(9-10), pp.1184-1194.

Strömberg, N. (1999): Finite element treatment of two-dimensional wear problems. *Computer Methods in Applied Mechanics and Engineering*, 177, pp.441-455.

Williams, J. A. (2001): Friction and wear of rotating pivots in mems and other small scale devices. *Wear*, 251(1-12), pp.965-972.

Zhao, S. M.; Hilmas, G. E.; Dharani, L. R. (2009): Numerical simulation of wear in a C/C composite multidisk clutch. *Carbon*, 47(9), pp.2219-2225.

